JCI The Journal of Clinical Investigation

Multisystem inflammatory syndrome in children is driven by zonulin-dependent loss of gut mucosal barrier

Lael M. Yonker, … , David R. Walt, Alessio Fasano

J Clin Invest. 2021;131(14):e149633. https://doi.org/10.1172/JCI149633.

Clinical Medicine | COVID-19 | Inflammation

Graphical abstract

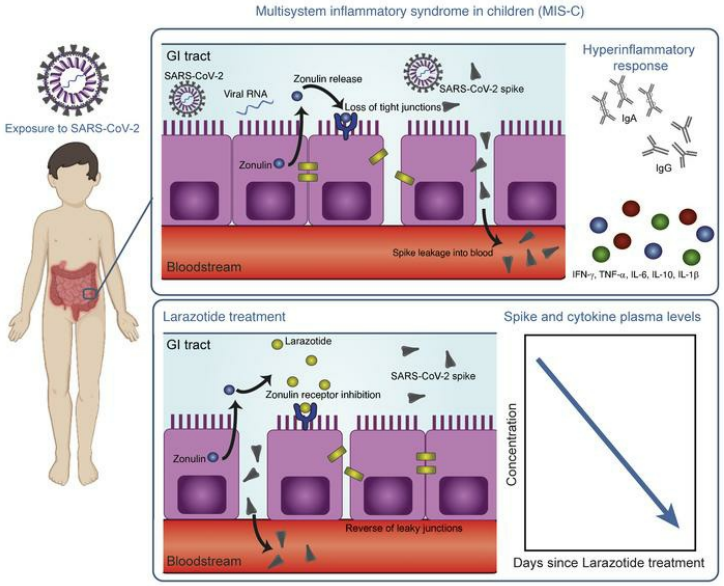

Find the latest version:

https://jci.me/149633/pdf

Multisystem inflammatory syndrome in children is driven by zonulin-dependent loss of gut mucosal barrier

Lael M. Yonker,[1,2,3] Tal Gilboa,[3,4,5] Alana F. Ogata,[3,4,5] Yasmeen Senussi,[4] Roey Lazarovits,[4,5] Brittany P. Boribong,[1,2,3] Yannic C. Bartsch,[3,6] Maggie Loiselle,[1] Magali Noval Rivas,[7] Rebecca A. Porritt,[7] Rosiane Lima,[1] Jameson P. Davis,[1] Eva J. Farkas,[1] Madeleine D. Burns,[1] Nicola Young,[1] Vinay S. Mahajan,[3,6] Soroush Hajizadeh,[3,8] Xcanda I. Herrera Lopez,[3,8] Johannes Kreuzer,[3,8] Robert Morris,[3,8] Enid E. Martinez,[1,3,9] Isaac Han,[3,5] Kettner Griswold Jr.,[3,5] Nicholas C. Barry,[3,5] David B. Thompson,[3,5] George Church,[3,5,10] Andrea G. Edlow,[3,11,12] Wilhelm Haas,[3,8] Shiv Pillai,[3,6] Moshe Arditi,[7] Galit Alter,[3,6] David R. Walt,[3,4,5] and Alessio Fasano[1,2,3,13]

[1]Mucosal Immunology and Biology Research Center and [2]Department of Pediatrics, Massachusetts General Hospital, Boston, Massachusetts, USA. [3]Harvard Medical School, Boston, Massachusetts, USA. [4]Department of Pathology, Brigham and Women's Hospital, Boston, Massachusetts, USA. [5]Wyss Institute for Biologically Inspired Engineering, Harvard University, Boston, Massachusetts, USA. [6]Ragon Institute of MIT, MGH and Harvard, Cambridge, Massachusetts, USA. [7]Department of Pediatrics, Division of Infectious Diseases and Immunology, Infectious and Immunologic Diseases Research Center (IIDRC) and Department of Biomedical Sciences, Cedars-Sinai Medical Center, Los Angeles, California, USA. [8]Massachusetts General Hospital Cancer Center, Boston, Massachusetts, USA. [9]Department of Anesthesiology, Critical Care and Pain Medicine, Boston Children's Hospital, Boston, Massachusetts, USA. [10]Department of Genetics, Harvard Medical School, Boston, Massachusetts, USA. [11]Department of Obstetrics and Gynecology, Division of Maternal-Fetal Medicine and [12]Vincent Center for Reproductive Biology, Massachusetts General Hospital, Boston, Massachusetts, USA. [13]European Biomedical Research Institute of Salerno (EBRIS), Salerno, Italy.

BACKGROUND. Weeks after SARS-CoV-2 infection or exposure, some children develop a severe, life-threatening illness called multisystem inflammatory syndrome in children (MIS-C). Gastrointestinal (GI) symptoms are common in patients with MIS-C, and a severe hyperinflammatory response ensues with potential for cardiac complications. The cause of MIS-C has not been identified to date.

METHODS. Here, we analyzed biospecimens from 100 children: 19 with MIS-C, 26 with acute COVID-19, and 55 controls. Stools were assessed for SARS-CoV-2 by reverse transcription PCR (RT-PCR), and plasma was examined for markers of breakdown of mucosal barrier integrity, including zonulin. Ultrasensitive antigen detection was used to probe for SARS-CoV-2 antigenemia in plasma, and immune responses were characterized. As a proof of concept, we treated a patient with MIS-C with larazotide, a zonulin antagonist, and monitored the effect on antigenemia and the patient's clinical response.

RESULTS. We showed that in children with MIS-C, a prolonged presence of SARS-CoV-2 in the GI tract led to the release of zonulin, a biomarker of intestinal permeability, with subsequent trafficking of SARS-CoV-2 antigens into the bloodstream, leading to hyperinflammation. The patient with MIS-C treated with larazotide had a coinciding decrease in plasma SARS-CoV-2 spike antigen levels and inflammatory markers and a resultant clinical improvement above that achieved with currently available treatments.

CONCLUSION. These mechanistic data on MIS-C pathogenesis provide insight into targets for diagnosing, treating, and preventing MIS-C, which are urgently needed for this increasingly common severe COVID-19–related disease in children.

Introduction

Most children who are acutely infected with SARS-CoV-2 develop mild upper respiratory symptoms or experience asymptomatic infection. Several days to weeks after resolution of the initial infection, some of these children will develop a severe life-threatening illness, termed multisystem inflammatory syndrome in children (MIS-C), which is an immune activation syndrome associated with prior SARS-CoV-2 infection or exposure. Patients with MIS-C present with persistent fever, marked gastrointestinal (GI) symptoms, cytokine storm, myocardial dysfunction, and cardiogenic shock with ventricular dysfunction in the setting of multisystem inflammation, reminiscent of, yet distinct from, toxic shock syndrome or Kawasaki disease (1). Eighty percent of these hospitalized children develop cardiac pathology (2), including coronary artery dilations, myocardial dysfunction, or ventricular failure with hypotensive shock (3). The cause of this late-phase severe illness in children has not previously been identified, leaving treatment options and prevention strategies nebulous. As the prevalence of SARS-CoV-2 infections among children and adolescents is increasing (4), MIS-C cases are increasing as well. A better understanding of this life-threatening illness is urgently needed.

Authorship note: LMY, TG, and AFO contributed equally to this work. DRW and AF contributed equally to this work.

Conflict of interest: AF is co-founder of and stockholder in Alba Therapeutics. DRW has a financial interest in Quanterix Corporation, developer of the ultrasensitive digital immunoassay platform. He is an inventor of the Simoa technology, a founder of the company, and also serves on its board of directors.

Submitted: March 15, 2021; **Accepted:** May 19, 2021; **Published:** July 15, 2021.
Reference information: *J Clin Invest*. 2021;131(14):e149633.
https://doi.org/10.1172/JCI149633.

Table 1. Age and sex for all pediatric patients and controls, and clinical features of illness for the children with acute COVID-19 or MIS-C

Total enrolled (n = 100)	MIS-C (n = 19)	COVID-19 (n = 26)	Controls (n = 55)	P value
Age, mean yr (max., min.)	8 (0.17, 21)	14 (2 wk, 22)	12 (2 mo, 20)	$P < 0.001$
Female sex, no. (%)	6 (32)	13 (50)	31 (56)	NS
Male sex, no. (%)	13 (68)	13 (50)	24 (44)	NS
Days since COVID-19/exposure, median (max, min)	26 (13, 62)	3 (0, 10)	NA	$P < 0.0001$
Days of MIS-C symptoms, median (max., min.)	3 (1, 28)	NA	NA	NA
Reported respiratory symptoms, no. (%)	7 (37)	19 (73)	NA	$P < 0.05$
Reported GI symptoms, no. (%)	17 (89)	7 (27)	NA	$P < 0.0001$

Significant differences between groups were assessed by 1-way ANOVA with Tukey's multiple-comparison test (age), χ^2 test (sex), Mann-Whitney t test (days since COVID-19 exposure), or Fisher's exact test (report of respiratory and GI symptoms). max., maximum; min., minimum.

Children with MIS-C display increased monocyte recruitment and hyperphagocytosis (5) with a cytokine storm (6), T cell activation (7), and inflammation driven by expansion of immunoglobulins (5, 8). A recently discovered superantigen-like motif near the S1/S2 cleavage site on the SARS-CoV-2 spike protein (9, 10) is hypothesized to drive this hyperinflammatory response in MIS-C. However, in most MIS-C cases, SARS-CoV-2 is undetectable by reverse transcription PCR (RT-PCR) of the nasopharyngeal swab, leaving the etiology and timing of this hyperinflammatory response yet to be elucidated (2, 11). In adults, there is increased recognition that the gut serves as a nidus for SARS-CoV-2 (12) and that in severe COVID-19, dysbiosis and disruption of the GI barrier drive inflammatory activation (13, 14). Although GI symptoms predominate MIS-C symptomatology (2), the role of the GI tract in the pathogenesis of MIS-C has not been evaluated.

In this study, we provide evidence that GI sources of SARS-CoV-2 viral antigenemia may instigate and drive MIS-C. We demonstrate that weeks after the initial infection, SARS-CoV-2 RNA remains in the GI tract, and zonulin-instigated hyperpermeability of the mucosal barrier coincides with SARS-CoV-2 antigenemia. Current treatment strategies are targeted at dampening the inflammatory response but do not address mucosal permeability or antigenemia. Here, we provide insight into the mechanism of disease pathogenesis and present evidence related to the trigger of MIS-C, thereby offering biomarkers for early detection of disease and avenues for the prevention and treatment of MIS-C.

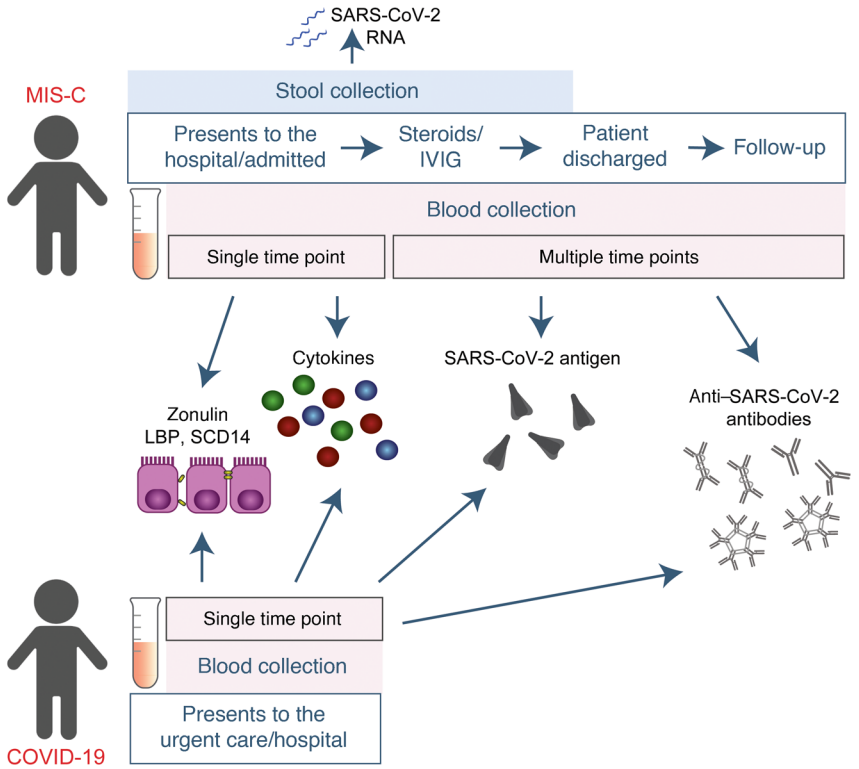

Figure 1. Study overview. Timing of sample collection and sample analysis for children with MIS-C or acute COVID-19.

Results

This study included biospecimens from 100 children: 19 children were clinically diagnosed with MIS-C as defined by CDC criteria (Supplemental Table 1; supplemental material available online with this article; https://doi.org/10.1172/JCI149633DS1); 26 children had COVID-19 confirmed by RT-PCR; and 55 children served as non–COVID-19 controls (32 pre-pandemic). The average age of the children with MIS-C (8 years old) was younger than that of the children who presented with COVID-19 (14 years old), which is consistent with the national averages (2, 15). The patients with MIS-C presented with a median of 3 days of acute symptoms associated with MIS-C (range, 1–28 days), after a previous COVID-19 exposure or SARS-CoV-2 infection 26 days prior to the presentation with MIS-C (range, 13–62 days). Notably, GI symptoms were predominant in the MIS-C cohort, affecting 89% of these patients, compared with 27% of children with acute COVID-19 (Fisher's exact test, $P < 0.0001$; Table 1). Figure 1 outlines the specimens collected for the analysis and the timing of specimen collection from the children with MIS-C or acute COVID-19.

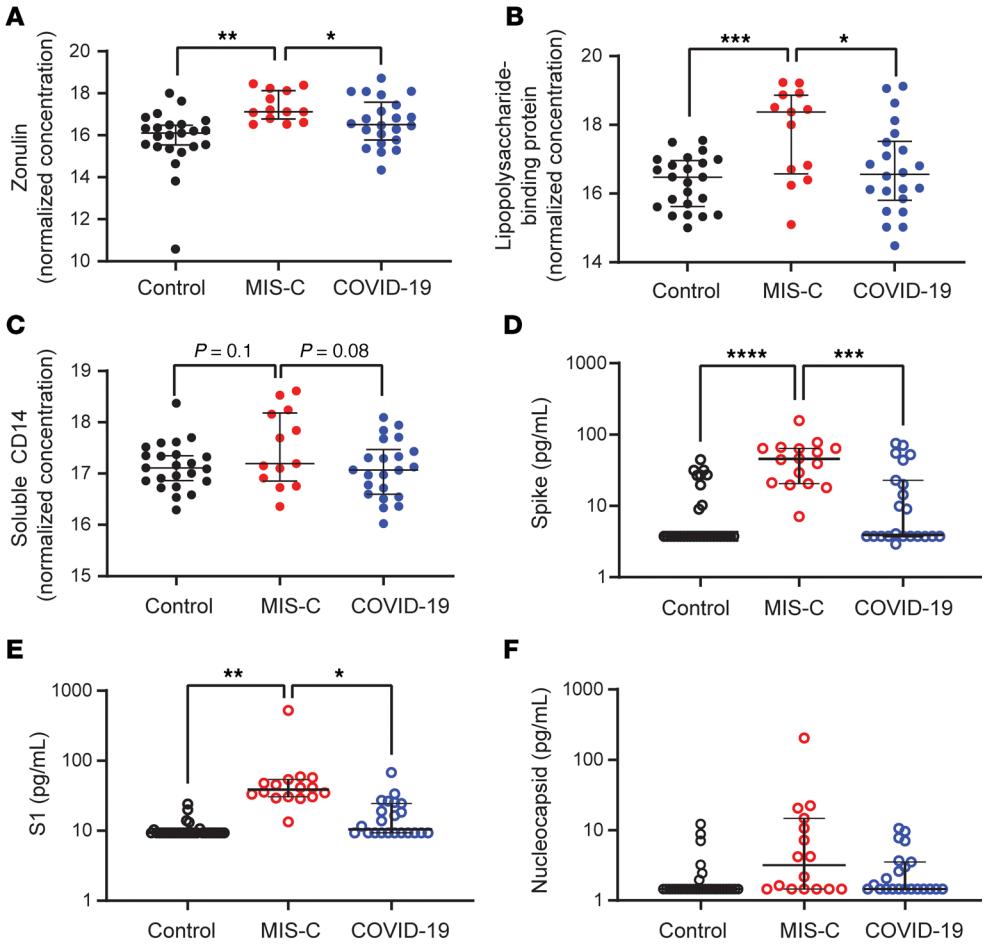

Figure 2. Plasma (**A**) zonulin, (**B**) LPS-binding protein, and (**C**) soluble CD14 levels were quantified by multiplexed MS–based proteomics (54, 55) for children with MIS-C (n = 13) or COVID-19 (n = 21) and for non–COVID-19 control participants (n = 23). Results were compared by ANOVA. (**D**) SARS-CoV-2 spike, (**E**) S1, and (**F**) nucleocapsid protein levels were quantified in plasma from children with MIS-C (n = 16), children with acute COVID-19 (n = 22), and pre-pandemic healthy controls (n = 32). Results were compared by 1-way ANOVA with multiple comparisons. * $P < 0.05$, ** $P < 0.01$, *** $P < 0.001$, and **** $P < 0.0001$. Median values and 95% CI are presented.

SARS-CoV-2 in the GI tract of children with MIS-C coincides with a loss of intestinal epithelial barrier function. MIS-C develops several weeks after a SARS-CoV-2 infection or exposure (Table 1), and the viral load in respiratory secretions is known to decrease over the course of 7–10 days after infection (11, 16, 17). As most children with MIS-C have negative nasopharyngeal viral swabs (11), MIS-C is unlikely to be related to this initial infection of the respiratory tract. To assess the presence of SARS-CoV-2 in the GI tract, we measured SARS-CoV-2 RNA from MIS-C stool samples collected several weeks after the initial SARS-CoV-2 infection or exposure. Indeed, a majority of the patients showed detectable viral loads in the stool ranging from 1.5×10^2 to 2.5×10^7 RNA copies/mL, suggesting an ongoing nidus of infection in MIS-C (Supplemental Table 1).

An intact, functional intestinal mucosal barrier should prevent the passage of large antigens from the gut lumen into the bloodstream, including viral antigens derived from SARS-CoV-2 present in the GI tract (12). Zonulin belongs to a family of structurally and functionally related proteins that reversibly regulate intestinal permeability by modulating intercellular tight junctions (18–20). Increased circulating zonulin levels resulting in increased intestinal permeability have been reported in several diseases (21) including autoimmune and hyperinflammatory diseases such as celiac disease (22), inflammatory bowel disease (23), and Kawasaki disease (24). Zonulin release from epithelial cells can result in permissibility of paracellular trafficking of large inflammatory antigens from the gut lumen into the bloodstream. In this study, mass spectrometry showed that, compared with controls, children with MIS-C had significantly increased release of zonulin into the circulation (P = 0.003; Figure 2A), which can result in a breakdown of mucosal barrier function. Correspondingly, children with MIS-C also had increased LPS-binding protein (LBP) levels compared with controls (P = 0.007; Figure 2B), signaling increased microbial translocation. Levels of soluble CD14, another marker of microbial translocation, were also increased in children with MIS-C (P = 0.1; Figure 2C), indicating a loss of GI mucosal barrier integrity. None of these markers of GI barrier integrity — zonulin, LBP, or CD14 — was significantly increased in the children with acute COVID-19 infection. Identification of SARS-CoV-2 within the stool, coupled with the loss of competency of tight junctions seen in MIS-C, but not acute COVID-19, suggests that GI sources of SARS-CoV-2 viral components could breach the mucosal barrier and enter the circulation.

Children with MIS-C have SARS-CoV-2 antigenemia. Although viremia and antigenemia have been shown to correlate with severe acute COVID-19 in adults (17, 25), viremia has not been detected in MIS-C (11), and antigenemia has not previously been assessed in children. Using single-molecule array (Simoa) assays (25), we detected SARS-CoV-2 spike, S1, and nucleocapsid antigens in the plasma of children with MIS-C despite being weeks past their initial SARS-CoV-2 infection or exposure. The SARS-CoV-2

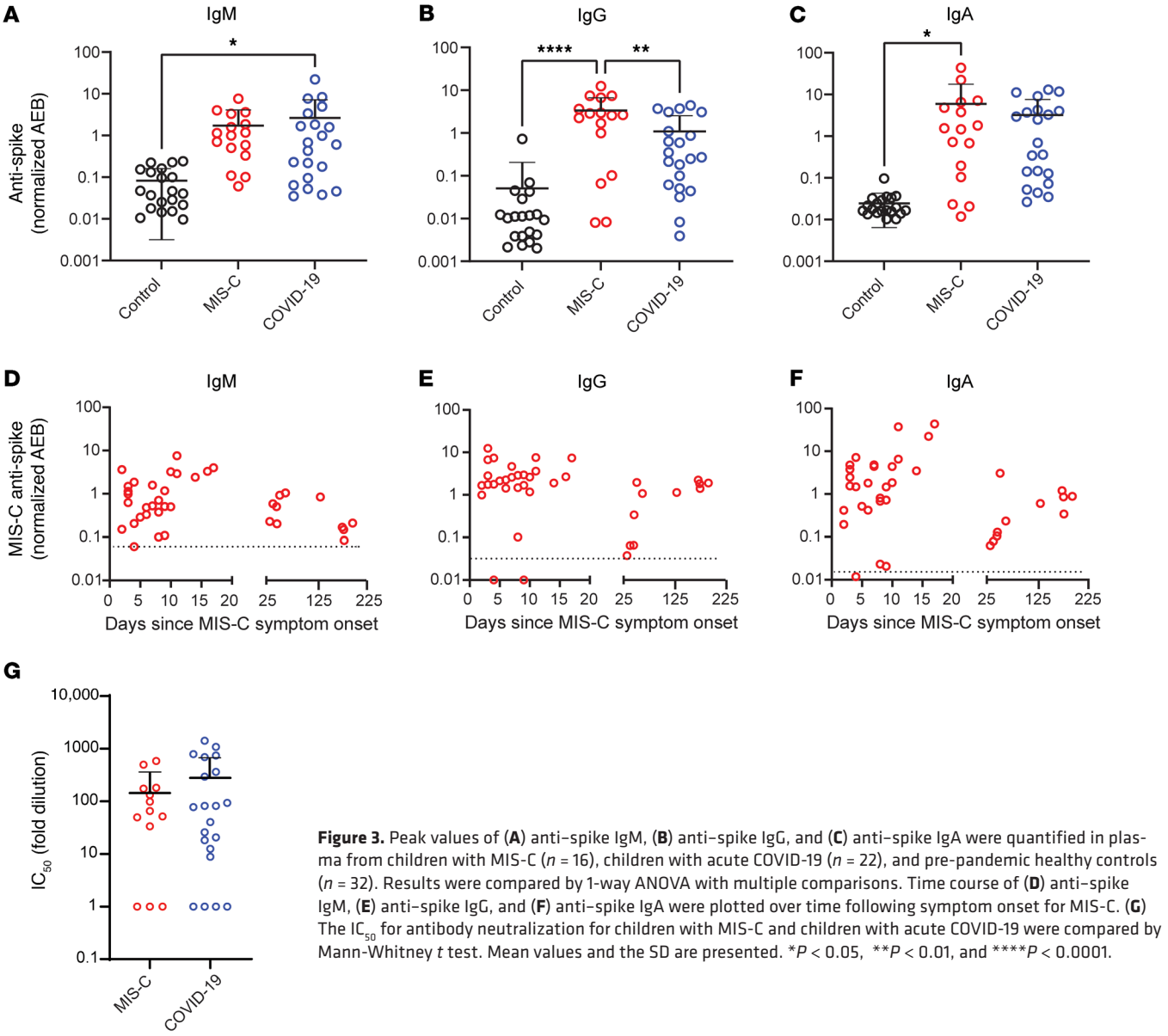

Figure 3. Peak values of (**A**) anti–spike IgM, (**B**) anti–spike IgG, and (**C**) anti–spike IgA were quantified in plasma from children with MIS-C (n = 16), children with acute COVID-19 (n = 22), and pre-pandemic healthy controls (n = 32). Results were compared by 1-way ANOVA with multiple comparisons. Time course of (**D**) anti–spike IgM, (**E**) anti–spike IgG, and (**F**) anti–spike IgA were plotted over time following symptom onset for MIS-C. (**G**) The IC_{50} for antibody neutralization for children with MIS-C and children with acute COVID-19 were compared by Mann-Whitney t test. Mean values and the SD are presented. *P < 0.05, **P < 0.01, and ****P < 0.0001.

spike protein was significantly elevated in patients with MIS-C compared with healthy controls (P < 0.0001) and compared with children with acute COVID-19 (P < 0.001; Figure 2D). We also detected the SARS-CoV-2 S1 protein at significantly elevated levels in patients with MIS-C compared with healthy controls (P = 0.004) and with children with acute COVID-19 (P = 0.02; Figure 2E). SARS-CoV-2 nucleocapsid protein levels were increased in patients with MIS-C, although these levels did not reach significance (Figure 2F). We detected no significant increase in SARS-CoV-2 antigenemia in children with acute COVID-19 as compared with healthy controls. SARS-CoV-2 antigens showed no correlation with age (Supplemental Figure 1). Circulating SARS-CoV-2 antigen indicates that viral components have leaked from infected tissues. We attribute circulating antigen in patients with MIS-C to leakage from the GI system, as corroborated by the increased zonulin levels and microbial translocation markers we detected in the patients with MIS-C.

The SARS-CoV-2 spike protein, specifically the S1 component (9, 10), has been hypothesized to have superantigen-like properties that are similar to those seen in the bacterial superantigen–mediated toxic shock syndrome. Superantigens bind to specific β-chains of T cell receptors (TCRs) at the variable domain in a complementary-determining region 3–independent (CDR3-independent) manner (26), thereby bypassing TCR specificity and resulting in skewing and overrepresentation of specific TCRs. Recent reports have identified TCR β variable (*TRBV*) gene skewing in MIS-C, with a profound expansion of TRBV11-2 (10, 27). Our data reveal a strong correlation between S1 antigenemia and the previously reported expression of TRBV11-2 in MIS-C (ref. 10; Pearson's correlation, r = 0.89, P = 0.0005; Supplemental Figure 2). We found no correlation between the spike or nucleocapsid antigens and TRBV11-2 expression (Supplemental Figure 2).

Consistent with hyperinflammatory responses, children with MIS-C experienced a cytokine storm with significantly elevated

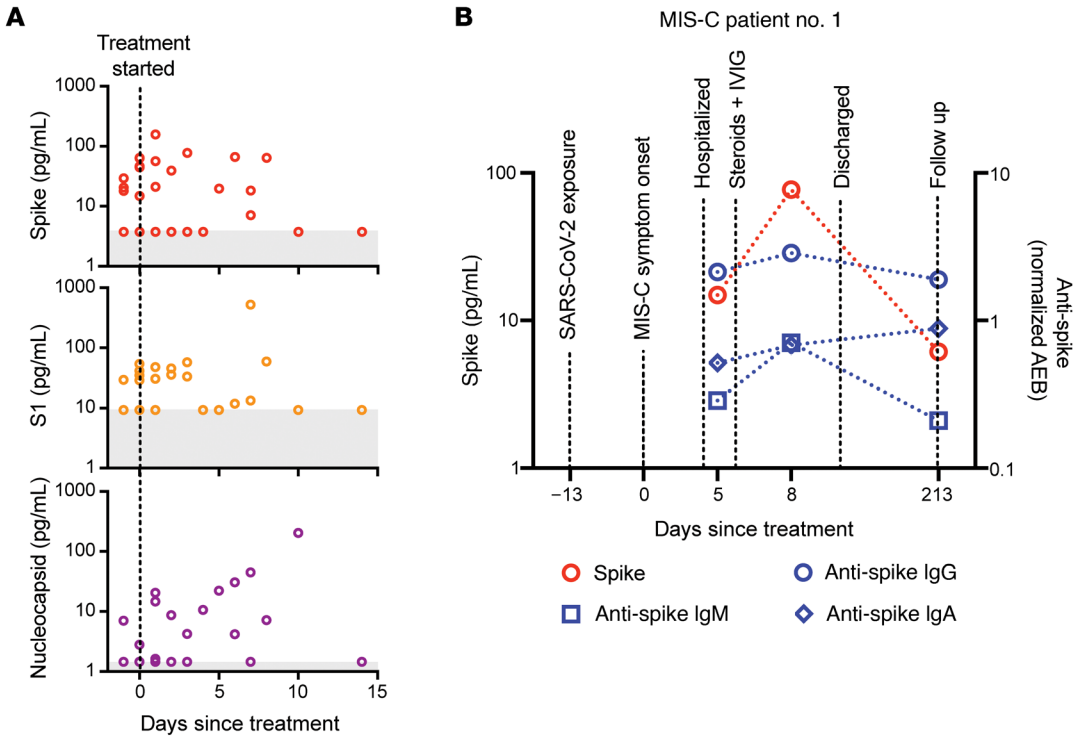

Figure 4. (**A**) SARS-CoV-2 spike, S1, and nucleocapsid levels in plasma from children with MIS-C were quantified before treatment with steroids and/or immunoglobulin replacement therapy, through 14 days following treatment (n = 11). Shaded regions signify the limit of detection for each specific antigen test. (**B**) Spike and anti–spike IgM, anti–spike IgG, and anti–spike IgA levels were measured over the course of illness of a child with MIS-C. Of note, the spike protein remained above the limit of detection for the spike antigen test at the 213-day follow-up point.

levels of IL-1β, IL-6, IL-10, and TNF-α (Supplemental Figure 3, A–D). Notably, the antiviral cytokine IFN-γ was also significantly increased in patients with MIS-C compared with both healthy controls and children with acute COVID-19 (Supplemental Figure 3E). This increase in IFN-γ is typical of a viral exposure, however, it can be paradoxically suppressed in adults with severe acute COVID-19 (28). We also assessed IL-12p70, IL-8, IL-5, and IL-22 levels but found that they were not altered in the children with MIS-C or acute COVID-19 (Supplemental Figure 3, F–I).

MIS-C immunoprofiles reflect ongoing mucosal exposure to SARS-CoV-2. The immunoglobulin IgM, IgG, and IgA subsets targeting SARS-CoV-2 antigens in patients with MIS-C were most highly elevated against spike and S1 proteins (Figure 3, A–C, and Supplemental Figure 4), corresponding to the antigens most highly detected in the bloodstream of these children. As expected, anti–spike IgM was highest in children with acute COVID-19, reflecting early adaptive immune responses (Figure 3A). However, anti–spike IgM levels remained higher than would be expected, given that MIS-C presents weeks after the original infection with or exposure to SARS-CoV-2, but was on a downward trend over time (Figure 3D). As expected, anti–spike IgG, anti–S1 IgG, and anti–RBD IgG were highest in the children with delayed-onset MIS-C (Figure 3B and Supplemental Figure 4) and remained plateaued over time (Figure 3E). IgA is the immunoglobulin most reflective of mucosal immunity and typically wanes following viral clearance (29). Here, the levels of anti–spike IgA, anti–S1 IgA, and anti–RBD IgA were all significantly increased in the patients with MIS-C (Figure 3C and Supplemental Figure 4), and anti–spike IgA remained unexpectedly elevated for months after the initial SARS-CoV-2 infection (Figure 3F). The persistence of elevated anti–SARS-CoV-2 IgA and IgM in patients with MIS-C supports the hypothesis of ongoing viral antigenic exposure and inflammation in the GI mucosal surfaces of children with MIS-C.

We compared the capacity of plasma neutralization against SARS-CoV-2 between children with MIS-C and those with acute COVID-19. Interestingly, although the children with MIS-C had significantly elevated IgG antibody titers against SARS-CoV-2 relative to those with acute COVID-19, the neutralization titers were comparable between the children from both groups (Figure 3G). This suggests that in children with MIS-C, increasing quantities of IgG antibodies against the SARS-CoV-2 spike protein did not result in a gain in neutralizing capacity over time. Ineffective neutralization and poor antigen clearance, combined with ongoing viral antigen leakage from GI sources, could partially explain the high levels of antigen detected in the children with MIS-C.

Temporal kinetics reveal that SARS-CoV-2 antigenemia is inadequately contained by humoral responses in MIS-C. Both SARS-CoV-2 antigen and immunoglobulins were detectable in patients with MIS-C at levels significantly higher than those detected in healthy controls. Antigenemia in adults occurs early in the COVID-19 disease course and is associated with pulmonary symptoms (25), whereas in MIS-C, antigenemia is found in the setting of prominent GI symptoms weeks to months after resolution of a SARS-CoV-2 upper respiratory tract infection or asymptomatic infection. To understand the relationship between viral antigenemia and the humoral response, we studied longitudinal samples from patients with MIS-C. First, we assessed

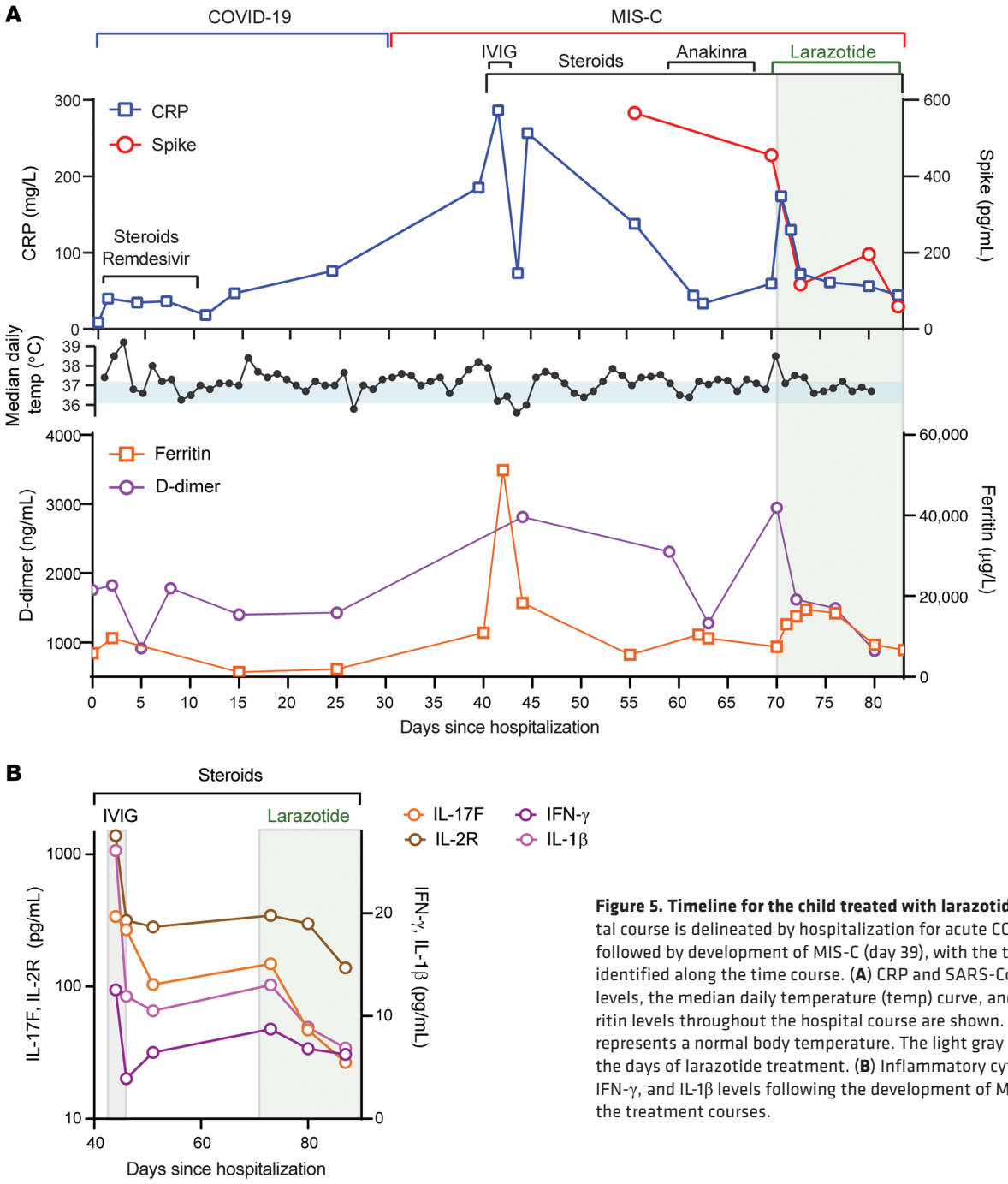

Figure 5. Timeline for the child treated with larazotide. The hospital course is delineated by hospitalization for acute COVID-19 (day 0) followed by development of MIS-C (day 39), with the treatment courses identified along the time course. (**A**) CRP and SARS-CoV-2 spike antigen levels, the median daily temperature (temp) curve, and D-dimer and ferritin levels throughout the hospital course are shown. Light blue shading represents a normal body temperature. The light gray shading highlights the days of larazotide treatment. (**B**) Inflammatory cytokine IL-17F, IL-2R, IFN-γ, and IL-1β levels following the development of MIS-C, in relation to the treatment courses.

antigens over time following MIS-C symptom onset. Previous reports show that in adults with acute COVID-19, SARS-CoV-2 antigens are rapidly cleared as the patient reaches seroconversion (25, 30). In contrast, our studies showed that spike antigens rose over the first few days of MIS-C symptoms and persisted for more than 10 days, occasionally through 6 months (Supplemental Figure 5), despite seroconversion to anti–spike IgG and anti–spike IgA antibodies. The elevated presence of spike protein in seroconverted patients was not observed in any adult COVID-19 cases (25). We also found that SARS-CoV-2 antigen levels did not significantly decrease in our cohort following the initiation of steroid and/or intravenous immunoglobulin (IVIG) replacement therapy (Figure 4A), which are the only currently recommended treatments for MIS-C (31). This suggests that current therapies are targeted toward the downstream consequences of MIS-C, namely the inflammatory responses, but fail to address the ongoing antigenemia instigating ongoing inflammation. Figure 4B provides a detailed overview of spike antigenemia and the humoral inflammatory responses in a representative hospitalized child with MIS-C, relative to SARS-CoV-2 exposure, symptom onset, and treatment course.

Zonulin antagonism reduces spike antigenemia and cytokine storm, with subsequent improvement in clinical outcomes in MIS-C. Although steroids and IVIG do not block leakage of SARS-CoV-2 antigen across the mucosal barrier, therapies targeting GI mucosal permeability could potentially reduce or prevent antigenemia.

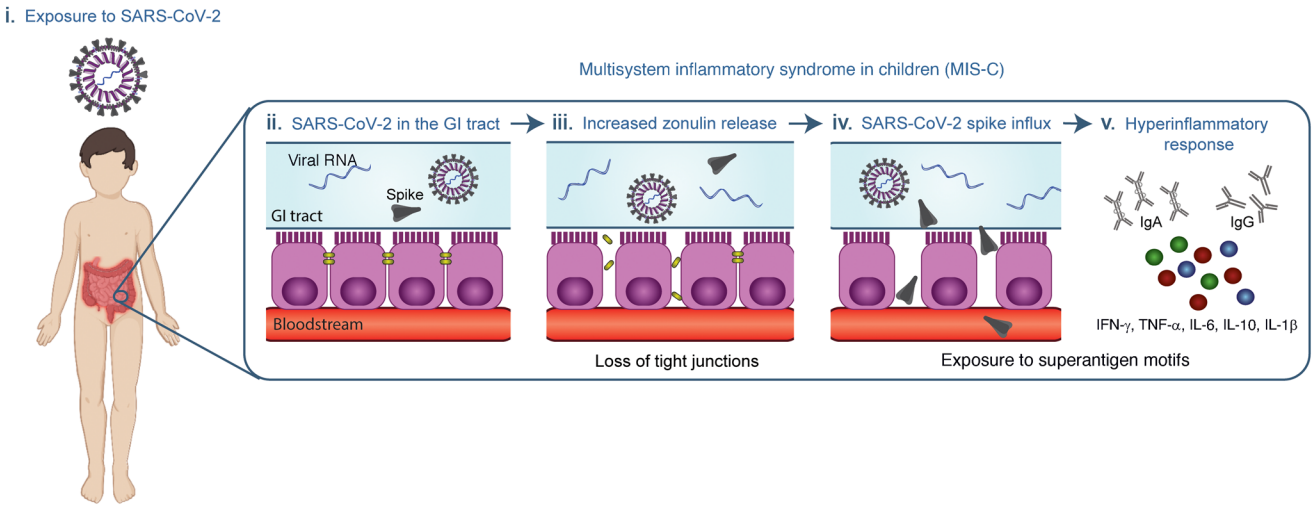

Figure 6. Overview of the proposed hypothesis that SARS-CoV-2 antigenemia drives MIS-C. (i) A child is exposed to or infected with SARS-CoV-2. (ii) SARS-CoV-2 enters the GI tract. (iii) Dysbiosis leads to increased zonulin release and a resultant loss of tight junctions. (iv) SARS-CoV-2 antigens, especially the spike protein, breaches the mucosal barrier and enters the blood stream. (v) The superantigen motif of the spike protein stimulates a pathogenic hyperinflammatory response.

Larazotide, a zonulin antagonist, is an investigational therapy that has been well characterized in preclinical trials (32, 33), with an excellent safety profile (34), and is currently in phase III trials for the treatment of refractory celiac disease (35). Given this theoretical benefit, we obtained US FDA approval for compassionate use of larazotide, 10 μg/kg every 6 hours, to treat a critically ill 17-month-old boy with MIS-C after he failed to improve with antiinflammatory therapies. The toddler, who had a complex past medical history including partial duplication of chromosome 14, biliary atresia status post Kasai procedure, and gastrotomy tube placement, with frequent episodes of ascending cholangitis, required hospitalization for severe COVID-19, complicated by respiratory failure and cardiac resuscitation. One month after he was diagnosed with COVID-19, he developed abdominal compartment syndrome with a C-reactive protein (CRP) level of 286 mg/L, a ferritin level of 51,223 μg/L, and a N-terminal pro-b–type natriuretic peptide (NT-proBNP) level of 16,462 pg/mL without evidence of cardiac injury on echocardiogram. He was treated with IVIG, steroids, and anakinra with transient improvement of inflammatory markers but rapid recrudescence of symptoms. We detected 1020 copies of SARS-CoV-2 RNA in the patient's stool, as quantified by RT-PCR, and a plasma spike antigen level of 566 pg/mL more than 2 weeks after initiation of IVIG and steroid treatment for MIS-C. After the initiation of larazotide, his CRP level, which had quickly rebounded to 173 mg/L following withdrawal of anakinra, dropped by 85% from peak values, and spike antigen levels dropped by 90% to 59 pg/mL (Figure 5A). The SARS-CoV-2 nucleocapsid protein levels also dropped by 98% from 77 pg/mL to 1.45 pg/mL (limit of detection). His fever curve, which also rebounded after discontinuation of anakinra, improved, as did his ferritin and D-dimer levels (Figure 5A). The patient also experienced an improvement in cytokine and inflammatory mediator levels, including IL-1β, IFN-γ, IL-2R, and IL-17, representing an improvement in inflammasome activation, virus-induced IFN release, and immune cell activation (Figure 5B). These cytokines and inflammatory mediators initially spiked during the development of MIS-C, then improved following IVIG but plateaued or rebounded despite steroid treatment. We observed an improvement in these inflammatory mediators following the precipitous drop in SARS-CoV-2 antigens, which occurred as a result of or coincident with the initiation of larazotide therapy. Importantly, the patient achieved his longest stretches without fever since his hospital admission, his GI symptoms improved and he was able to resume full feedings, and his ventilatory status improved.

Discussion

Although children were initially considered to be relatively spared from COVID-19, it is now evident that they can become infected with SARS-CoV-2 but show only minimal or no symptoms during the acute infection stage (11). The prevalence of COVID-19 in children and adolescents has climbed over the past few months (4, 36). As a result, the incidence of MIS-C, once reported to be a life-threatening but rare late manifestation, is also increasing. Identifying children early in the disease course of MIS-C, before cardiac complications ensue, is critical, and a dire need exists to understand the pathogenesis driving MIS-C to treat and prevent this increasingly prevalent disease in children. The data provided here represent the first evidence to our knowledge of prolonged exposure to SARS-CoV-2 in the GI tract of children with MIS-C coinciding with zonulin release, indicating a loss of mucosal barrier integrity, and SARS-CoV-2 antigenemia, which may be driving the hyperinflammatory responses defining MIS-C (Figure 6). Further, as a proof of concept, we show that inhibition of intestinal permeability in a patient with MIS-C prevented SARS-CoV-2 antigens from trafficking into the bloodstream, conferring clinical benefit by addressing the underlying trigger for MIS-C rather than just the inflammatory consequences.

SARS-CoV-2 antigenemia has not previously been reported in MIS-C. Although epidemiologically linked to a prior SARS-CoV-2 infection, previous studies have been unable to attribute MIS-C

to viremia (11). In contrast, 77% of adults with severe COVID-19 requiring intensive care unit (ICU) admission for respiratory failure were found to have plasma SARS-CoV-2 antigenemia (25), which was believed to originate from respiratory sources (25). Nucleocapsid and S1 antigens were the most prominent SARS-CoV-2 antigens detected in the blood of adults with severe COVID-19. In children with MIS-C, the spike and S1 protein are the predominant antigens. The difference in makeup of SARS-CoV-2 antigenemia warrants further investigation, as this could provide insight into differences between MIS-C and severe adult COVID-19.

The S1 subunit of the spike protein (S1), which is seen at significantly elevated levels in MIS-C, contains the superantigen-like motif that can interact with TCRs and MHC-II to trigger superantigenic responses leading to skewed TCR repertoire in MIS-C patients with expansion of the *TCRBV* gene (9, 10). Further, the SARS-CoV-2 superantigen–like motif was found to have remarkable sequence and structural similarity to the *Staphylococcus exotoxin B* (SEB) superantigen motif that interacts with both the TCR and CD28 (37) and mediates toxic shock syndrome. Here, we show, for the first time to our knowledge, a direct correlation between S1 antigenemia and the specific TRBV11-2 skewing seen in MIS-C.

The gut is the likely source of the antigenemia in MIS-C. MIS-C develops days to weeks after resolution of the initial infection, often when SARS-CoV-2 viral levels are low or undetectable in respiratory secretions (11), making the MIS-C trigger less likely to be from upper respiratory tract sources. In adults with COVID-19, SARS-CoV-2 can be detected in the stool (38) and on intestinal biopsies (39), with anti–SARS-CoV-2 IgA levels remaining elevated for over 4 months after the acute infection. These findings suggest that the GI tract may serve as a nidus for SARS-CoV-2 with ongoing immune activation (12). Further, an increased severity of acute COVID-19 in adults is associated with a greater frequency of GI symptoms (40). In our cohort of patients with MIS-C, the majority of stool samples from children with MIS-C contained SARS-CoV-2 RNA, and most MIS-C patients presented with unusually severe GI symptoms, abdominal pain, vomiting, and diarrhea, in addition to severe myocardial dysfunction and cardiac shock. Although extensive tissue studies are necessary to provide direct evidence of SARS-CoV-2 infection in the GI tract, these data, in addition to the predominance of severe GI symptoms in patients with MIS-C, point to a viral or viral antigenic source that originates from the GI system at the time of MIS-C presentation. Research is needed to better understand what the impact of the GI environment is on the SARS-CoV-2 virus and superantigen-like viral motifs, and why children are more likely than adults to develop antigenemia weeks after the acute infection.

Increased zonulin levels indicate a breakdown of intestinal epithelial tight junctions, which may allow the leak of SARS-CoV-2 antigen into the bloodstream. Zonulin is a modulator of intercellular epithelial tight junctions; various stimuli, including dysbiosis (41), activate MyD88-dependent zonulin release, allowing zonulin to bind to its target protease-activated receptor 2 (PAR2) and transactivate the EGFR (42). This triggers downstream signaling that leads to phosphorylation of tight junction proteins, including zonula occludens 1 (ZO1) and myosin 1c, ultimately causing disassembly of tight junctions and increased paracellular permeability to macromolecules (43). This mechanism has already been described for a variety of other chronic inflammatory diseases (44). In a murine model of Kawasaki disease vasculitis, increased intestinal permeability has been associated with higher levels of circulating IgA and its deposition in cardiovascular lesions (24). Blocking intestinal permeability in this murine model of Kawasaki disease with the zonulin inhibitor AT1001 (larazotide acetate, currently in a phase III clinical trial for celiac disease) significantly reduced the development of cardiovascular lesions, suggesting a possible involvement of zonulin in this process (24). A similar mechanistic link between zonulin-dependent spike protein trafficking from the GI tract into the bloodstream in MIS-C pathogenesis was further supported by our successful use of larazotide acetate in a toddler with MIS-C, described here. Following the initiation of larazotide, blood spike protein levels decreased by 90%, ameliorating inflammation and improving MIS-C–related symptoms in this patient. Similarly, in Kawasaki disease, patients presenting with prominent GI symptoms at the onset of illness are less likely to respond to IVIG therapy alone and thus more likely to develop coronary artery aneurysms (45). Here, we show that elevated levels of zonulin in MIS-C indicated increased permeability in the setting of SARS-CoV-2 detection in the stool.

We also show an increase of translocation of microbial factors in MIS-C that was not seen in the children with acute COVID-19, signifying an increased breakdown of GI barrier integrity in MIS-C. Although it is possible that these microbial factors contribute to the general inflammatory state of MIS-C, other diseases associated with increased translocation of microbial factors (46, 47) lack the distinct clinical symptomatology and pathology of MIS-C. This suggests that the intestinal leakage of the SARS-CoV-2 antigens themselves is responsible for triggering the profound cytokine release and hyperinflammatory response seen in MIS-C.

As zonulin-dependent loss of gut integrity develops in MIS-C– but not COVID-19–infected children, this suggests that a chronicity of SARS-CoV-2 dysbiosis in the gut results in a cumulative increase in the breakdown of mucosal barrier integrity. Additionally, this suggests that intervening and preventing mucosal epithelial damage early in the disease course could prevent the development of MIS-C. Larger, prospective studies are needed to better define the development of dysbiosis in MIS-C.

Analysis of the kinetic profile of the spike protein in patients with MIS-C showed that antigen leakage increased over time after the onset of MIS-C symptoms. Humoral responses alone are ineffective at controlling elevated levels of antigen in MIS-C and, in fact, contribute to the inflammatory profile (5). We show that in MIS-C, antibodies, especially anti–spike IgM and anti–spike IgA, continued to rise in response to antigen, suggesting ineffective adaptive immunity in addition to ongoing antigen release as a result of increased intestinal permeability. These data support previous reports of an expansion of inflammatory antibodies that are generated (5) for multiple non–COVID-19 pathogens, including common coronaviruses, influenza, and respiratory syncytial virus (RSV) (11), plus numerous self-antigens (8, 48), which in turn activate monocytes and elicit hyperphagocytosis (5), macrophage activation, and cytokine storm (6, 7). Of note, the assays used in our experiments detect the spike protein S1–S2 extracellular sub-

units but cannot not distinguish between live or dead virus. However, viral antigens can drive hyperinflammatory responses, and live virus is not required to induce an immune response.

Importantly, antigen levels persist for days to weeks after hospitalization and treatment for MIS-C in some cases, revealing that current treatments (i.e., steroids and/or IVIG) target inflammatory responses but may not adequately mitigate intestinal permeability and SARS-CoV-2 antigen leakage into the blood. This prolonged antigen leakage may explain the recrudescence of symptoms in some children and justify the rationale for a prolonged tapering of immunomodulatory therapies in MIS-C (49). Additionally, detection of bloodborne antigen and zonulin within the first few days of MIS-C symptom onset could identify those at risk for developing MIS-C. Conversely, increased levels of zonulin in children recently infected with SARS-CoV-2 may identify individuals at increased risk for developing MIS-C. Here, we show the proof of concept that zonulin antagonism directly reduced SARS-CoV-2 antigenemia with abatement of the cytokine storm and subsequent clinical improvement in a single patient. Although clinical trials will be needed to test whether larazotide is effective at treating or preventing MIS-C, this study highlights the proof of concept that, in a single patient, zonulin antagonism reduced SARS-CoV-2 antigenemia, improved inflammatory marker levels, and led to defervescence and clinical stabilization following treatment initiation. Diagnostic and therapeutic strategies aimed at targeting intestinal permeability could offer a new avenue for identifying, treating, or preventing MIS-C.

Conclusion. Here, we report what we believe to be compelling evidence that in MIS-C, zonulin-dependent loss of GI tight junctions results in SARS-CoV-2 antigenemia, driving hyperinflammatory immune activation. These data suggest that in MIS-C, the presence of SARS-CoV-2 in the GI tract may lead to local mucosal inflammation, increased zonulin release, and a subsequent increase in gut permeability allowing SARS-CoV-2 antigens, including the superantigen-like motif of the spike protein, to traffic across mucosal barriers and into the bloodstream. The data shown here advance our understanding of MIS-C pathogenesis, revealing potential biomarkers for MIS-C diagnosis as well as prospective pathways for treating and preventing MIS-C, all of which are urgently needed for this new and increasingly common life-threatening disease in children.

Methods

Antigen Simoa assays. SARS-CoV-2 antigen Simoa assays were prepared and performed using commercial antibodies for spike assays (Sino Biological, 40590-T62), S1 assays (Sino biological, 40150-D001), and nucleocapsid assays (Sino Biological, 40143-R004, 40143-R040), as well as a custom antibody for S1 as previously described (25). Plasma samples were diluted 8-fold in Homebrew Detector/Sample Diluent (Quanterix) with Halt Protease Inhibitor Cocktail (Thermo Fisher Scientific) and EDTA. Detector antibodies were diluted to 0.3 μg/mL in Homebrew Detector/Sample Diluent, and streptavidin-β-galactosidase (SβG) concentrate (Quanterix) was diluted to 150 pM in SβG Diluent (Quanterix). Antibody-conjugated capture beads were diluted in Bead Diluent (Quanterix), with a total of 500,000 beads per reaction (125,000 S1 beads, 125,000 S2 beads, 250,000 647 nm dye-encoded helper beads for the S1/S2 multiplex assay, and 125,000 nucleocapsid beads and 375,000 647 nm dye-encoded helper beads for the nucleocapsid assay). All reagents were diluted in plastic bottles that were loaded into the HD-X Analyzer (Quanterix). The assays were performed on an HD-X Analyzer in an automated 3-step assay format according to the manufacturer's instructions and as previously described (50). In each assay, capture beads were incubated with the sample for 15 minutes, with detector antibody for 5 minutes, and with SβG for 5 minutes, with washing steps in between. The beads were then resuspended in 25 μL resorufin-β-galactopyranoside and loaded into the microwell array for imaging. Average enzymes per bead (AEB) and sample concentration values were calculated using HD-X Analyzer software. All samples were measured in duplicate.

Multiplexed quantitative plasma proteomics. Protein concentration in plasma samples was determined using a BCA assay, and 100 μg plasma per sample was denatured in 6 M guanidinium chloride for 5 minutes at 95°C. Disulfide bonds were reduced and free thiols alkylated as previously described (51). Proteins were purified using solid-phase–enhanced sample preparation (SP3) technology with a 1:1 mixture of hydrophobic and hydrophilic Sera-Mag Speed Beads (GE Life Sciences) essentially as previously described (52), including sequential digestion with Lys-C and trypsin. For multiplexed quantification, peptides were labeled with TMT16 reagents (Thermo Fisher Scientific; refs. 53, 54). Samples were then combined into pools of 15 samples and 1 bridge sample generated by combining plasma proteome digests prior to tandem mass tag (TMT) labeling and used for quantitative comparison across TMT sets (54). The combined sample pools were fractionated using high-pH reversed-phase (HPRP) chromatography as previously described (51). Twelve fractions per sample were analyzed in 3-hour runs via reversed-phase liquid chromatography tandem mass spectrometry (LC-MS2/MS3) on either an Orbitrap Fusion Lumos or an Orbitrap Eclipse mass spectrometer using the simultaneous precursor selection–supported (SPS-supported) MS3 method (55, 56) essentially as described previously (57) and using Real-Time Search when using the Orbitrap Eclipse (58). MS2 spectra were assigned using a SEQUEST-based (59) in-house–built proteomics analysis platform (60) using a target-decoy database search strategy to assist filtering for a FDR of protein identifications of less than 10 % (61). Searches were done using the UniProt human protein sequence database (UP000005640; ref. 60). Only MS3 results with an average signal-to-noise value above 10 per reporter ion as well as with an isolation specificity (55) of greater than 0.75 were considered for quantification. Zonulin (pre-haptoglobin, HOY300), LPS-binding protein and soluble CD14 were quantified. Protein concentration data were normalized as previously described (54). A 1-way ANOVA was performed to compare relative protein concentrations between COVID-19, MIS-C, and healthy control samples. If the ANOVA showed significance with a P value of less than 0.05, a 2-sided t test was performed on paired sample groups to determine which proteins varied significantly between cohorts.

TCR immunosequencing. TCR immunosequencing and analysis of the MIS-C patients included here were originally performed at Cedars-Sinai Medical Center, as recently reported (10). Briefly, RNA was isolated from the peripheral blood of control participants and patients with MIS-C and assessed for quality with a bioanalyzer (Agilent Technologies). Sequencing of the TCR genes was performed using the QIAseq Immune Repertoire RNA Library Kit (QIAGEN) and

the NovaSeq 6000 system (Illumina; 2 × 250 bp, 11 M average reads per sample) as reported earlier (10). For analysis, the MiXCR framework (version 3.0.8) was used for annotation of the TCR rearrangements and clone construction, whereby the default MiXCR library served as a reference for sequence alignment, and each unique CDR3 nucleotide sequence was defined as 1 clone. Only productive sequences with a read count of 2 or higher were considered for further analysis as detailed previously (10).

Immunoglobulin Simoa assays. SARs-CoV-2 serological Simoa assays for IgA, IgM, and IgG against the 4 viral antigen S1, spike, nucleocapsid, and RBD were prepared and preformed using commercial antibodies for IgG assays (Bethyl Laboratories, A80-148B), IgM assays (Thermo Fisher Scientific, MII0401), and IgA assays (Abcam, ab214003) as previously described (30). Plasma samples were diluted 4000-fold in Homebrew Detector/Sample Diluent (Quanterix). Four antigen-conjugated capture beads were mixed and diluted in Bead Diluent, with a total of 500,000 beads per reaction (125,000 of each bead type). Biotinylated anti–human immunoglobulin antibodies were diluted in Homebrew Detector/Sample Diluent to final concentrations of 7.73 ng/mL IgG (Bethyl Laboratories, A80-148B); 216 ng/mL IgM (Thermo Fisher Scientific, MII0401); and 150 ng/mL IgA (Abcam, ab214003). SβG concentrate (Quanterix) was diluted to 30 pM in SβG Diluent (Quanterix). The serology assay was performed on an HD-X Analyzer (Quanterix) in an automated 3-step assay. AEB values were calculated by the HD-X Analyzer software and converted to normalized antibody titers using 4 calibrators that were included in each HD-X run.

Seroconversion classification was based on the early-stage classification model trained using an independent panel of 142 positive samples by RT-PCR SARS-Cov-2 and 200 negative pre-pandemic controls. The markers for this model were chosen using a cross-validation step. This cross-validation yielded 4 markers (IgA S1, IgA nucleocapsid, IgG nucleocapsid, and IgG spike) and had the best performance in the training set. The threshold for a positive test result for the unknown samples was determined on the basis of the cutoff that yielded 100% specificity in the training set (30).

Cytokine assays. Cytokines were measured in plasma samples using the CorPlex Cytokine Panel (Quanterix), which included sample diluent buffer. Plasma samples were diluted 4-fold in sample diluent buffer, and assays were performed following CorPlex protocols. Each CorPlex cytokine panel kit was analyzed by the SP-X Imaging and Analysis System (Quanterix).

Neutralization assay. The SARS-CoV-2 spike protein was pseudotyped onto a GFP expression–driving lentivirus reporter vector, similar to a previously published protocol (62). In order to improve trafficking to the cell membrane for the generation of virus-like particles (VLPs), 21 amino acids thought to contain a cryptic endoplasmic reticulum (ER) retention signal (63) were removed from the cytoplasmic tail, but the extracellular domain was left intact. Plasma samples were heat inactivated at 58°C for 1 hour, and a dilution series was created by performing 5-fold serial dilutions in cell culture medium (DMEM plus 10% FBS, 1% penicillin/streptomycin) beginning with a 1:50 dilution. Dilutions were then incubated with CoV-2 spike pseudotyped VLPs for 1 hour at 37°C before seeding modified ACE2-expressing human embryonic kidney 293 T (HEK293T) cells into the solution. Cells were incubated for 48 hours before trypsinization and fixation (4% paraformaldehyde for 30 minutes) prior to flow cytometric analysis. ACE2-expressing HEK293T cells were generated by integration of a separate hEf1a-hACE2 lentiviral vector at high MOI prior to FACS for expression of hACE2. hACE2 expression was found to be stable at 95% for more than 12 passages after FACS.

Neutralization capacities for plasma samples were determined by measuring the inhibition of GFP production in ACE2-expressing HEK293T cells as a function of plasma dilutions. The relative quantification of GFP^+ cells was determined by flow cytometry, and the quantities of GFP-expressing cells were normalized to the highest dilution of plasma. Neutralizing antibody titers at 50% inhibition (NT50) were calculated as the dilution corresponding to a normalized signal of 0.5 (i.e., 50% inhibition of GFP expression).

SARS-CoV-2 viral RNA detection. RNA was extracted from 100–200 μL stool using TRIzol (Thermo Fisher Scientific, 15596026) following the manufacturer's protocol. RNA was isolated from the collected aqueous layer using the RNeasy PowerMicrobiome Kit (QIAGEN, 26000-50) and eluted in 50 μL RNase-free water. Viral RNA was quantified as previously reported (64). In brief, the Luna Universal Probe One-Step RT-qPCR kit (New England BioLabs) was used, with CDC N1 primers (65) (Integrated DNA Technologies [IDT]) targeting the N gene of SARS-CoV-2: forward, GACCCCAAAATCAGCGAAAT; reverse, TCTGGTTACTGCCAGTTGAATCTG; probe, FAM-ACCCCGCATTACGTTTGGTGGACC-BHQ1. SARS-CoV-2 synthetic RNA molecules (Twist Bioscience) were included on the same RT-qPCR plate for each run, read out by a CFX96 Real-Time Detection System (Bio-Rad). Viral RNA content in each sample was quantified using the equation RNA copies = 1000 × 2^(ΔCt), where ΔCt is the difference between the cycle threshold of the RNA control and a given sample.

Statistics. Multiple comparisons were done using 1-way ANOVA with Tukey's multiple-comparison test, and dichotomous comparisons were made using the Mann-Whitney *t* test. Fisher's exact and χ^2 tests were used to analyze categorical differences between groups. A *P* value of less than 0.05 was considered significant. All data fittings and statistical tests were performed in GraphPad Prism 9 (GraphPad Software). All figures were plotted in GraphPad Prism 9 and Adobe Illustrator, version 2015.

Study approval. The participants, including the patient treated with FDA-approved emergency authorization of larazotide, were enrolled in either the IRB-approved Pediatric COVID-19 Biorepository (MGB no. 2020P000955) or the Pediatric Biorepository (MGB no. 2016P000949) at Massachusetts General Hospital after informed consent, and assent when appropriate, was obtained. Blood, nasopharyngeal swabs, oropharyngeal swabs, and stool samples were collected from children in the Pediatric COVID-19 Biorepository and processed as previously described (66). Demographics, past medical history, and clinical laboratory results were obtained from the patient's medical record. Serum samples were obtained from children enrolled in the Pediatric Biorepository. All procedures were approved by the Massachusetts General Hospital IRB. Hospitalized pediatric patients were defined as having MIS-C if they met the following CDC criteria (65): fever, laboratory evidence of inflammation, evidence of more than 2 organs affected, plus evidence of SARS-CoV-2 infection (current or recent nasopharyngeal RT-PCR–positive result for SARS-CoV-2 or positive SARS-CoV-2 serology) or exposure to an individual with confirmed or suspected COVID-19 within the past 4 weeks. Patients with a positive nasopharyngeal SARS-CoV-2 RT-PCR test without signs of MIS-C were defined as having acute COVID-19.

Author contributions

LMY, TG, AFO, DRW, and AF conceptualized the study and designed the methodology. LMY, TG, AFO, R. Lazarovits, R. Lima, BPB, YCB, ML, MNR, RAP, IH, JPD, EJF, MDB, NY, DBT, KG, NCB, VSM, SH, XIHL, JK, RM, EEM, WH, SP, and YS performed studies. LMY, TG, AFO, R. Lazarovits, BPB, MNR, RAP, MA, AGE, DRW, AF, SH, EEM, WH, and SP performed formal analysis. LY, TG, AFO, and AF wrote the manuscript. LY, TG, AFO, RL, GC, MA, GA, DRW, and AF reviewed and edited the manuscript and supervised the study.

Acknowledgments

We thank Aleksandra Binek and Angela McArdle for their technical support and measurements of zonulin and haptoglobin levels by proteomics at the Cedars-Sinai Medical Center Proteomics and Metabolomic core facility. This work was funded by the Erika Glazer COVID-19 Foundation. This research was also supported by the National Heart, Lung, and Blood Institute (NHLBI), NIH (5K08HL143183, to LMY); the National Institute of Diabetes and Digestive and Kidney Diseases (NIDDK), NIH (DK104344, to AF); the Regione Campania Italy (CUP G58D20000240002 - SURF 20004BP000000011, to AF); the NIH (3R01AI072726-10S1, to MA); and the Department of Pediatrics at Massachusetts General Hospital for Children (to LMY). Funding for the SARS-CoV-2 antigen measurements came from generous donations from Barbara and Amos Hostetter and the Chleck Foundation, and this work was supported in part by the Bill and Melinda Gates Foundation (no. INV-017380). FDA-approved compassionate use of larazotide was provided by 9 Meters Biopharma.

Address correspondence to: Alessio Fasano or Lael Yonker, Massachusetts General Hospital, 55 Fruit St., Jackson 14, Boston, Massachusetts 02114, USA. Phone: 617.726.1450; Email: afasano@mgh.harvard.edu (AF); Phone: 617.724.2890; Email: Lyonker@mgh.harvard.edu (LY). Or to: David Walt, Brigham and Women's Hospital, 60 Fenwood Rd., Boston, Massachusetts 02115, USA. Phone: 857.307.1112; Email: dwalt@bwh.harvard.edu.

1. Rowley AH, et al. Immune pathogenesis of COVID-19-related multisystem inflammatory syndrome in children. *J Clin Invest*. 2020;130(11):5619–5621.
2. Feldstein LR, et al. Multisystem inflammatory syndrome in U.S. children and adolescents. *N Engl J Med*. 2020;383(4):334–346.
3. Belhadjer Z, et al. Acute heart failure in multisystem inflammatory syndrome in children (MIS-C) in the context of global SARS-CoV-2 pandemic. *Circulation*. 2020;142(5):429–436.
4. MMWR. COVID-19 stats: COVID-19 incidence,* by age group(dagger) - United States, March 1–November 14, 2020(section sign). *MMWR Morb Mortal Wkly Rep*. 2021;69(5152):1664.
5. Bartsch YC, et al. Humoral signatures of protective and pathological SARS-CoV-2 infection in children. *Nat Med*. 2021;27(3):454–462.
6. Pierce CA, et al. Immune responses to SARS-CoV-2 infection in hospitalized pediatric and adult patients. *Sci Transl Med*. 2020;12(564):eabd5487.
7. Carter MJ, et al. Peripheral immunophenotypes in children with multisystem inflammatory syndrome associated with SARS-CoV-2 infection. *Nat Med*. 2020;26(11):1701–1707.
8. Gruber CN, et al. Mapping systemic inflammation and antibody responses in Multisystem Inflammatory Syndrome in Children (MIS-C). *Cell*. 2020;183(4):982–995.
9. Cheng MH, et al. Superantigenic character of an insert unique to SARS-CoV-2 spike supported by skewed TCR repertoire in patients with hyperinflammation. *Proc Natl Acad Sci U S A*. 2020;117(41):25254–25262.
10. Porritt RA, et al. HLA class I-associated expansion of TRBV11-2 T cells in Multisystem Inflammatory Syndrome in Children. *J Clin Invest*. 2021;131(10):e146614.
11. Yonker LM, et al. Pediatric SARS-CoV-2: clinical presentation, infectivity, and immune responses. *J Pediatr*. 2020;227:45–52.
12. Gaebler C, et al. Evolution of antibody immunity to SARS-CoV-2. *Nature*. 2021;591(7851):639–644.
13. Giron LB, et al. Severe COVID-19 is fueled by disrupted gut barrier integrity [preprint]. https://doi.org/10.1101/2020.11.13.20231209. Posted on medRxiv November 16, 2020.
14. Trottein F, Sokol H. Potential causes and consequences of gastrointestinal disorders during a SARS-CoV-2 infection. *Cell Rep*. 2020;32(3):107915.
15. CDC. Information for Healthcare Providers about Multisystem Inflammatory Syndrome in Children (MIS-C). https://www.cdc.gov/mis-c/hcp/. Updated February 17, 2021. Accessed May 20, 2021.
16. Wang Y, et al. Kinetics of viral load and antibody response in relation to COVID-19 severity. *J Clin Invest*. 2020;130(10):5235–5244.
17. Fajnzylber J, et al. SARS-CoV-2 viral load is associated with increased disease severity and mortality. *Nat Commun*. 2020;11(1):5493.
18. Fasano A, et al. Zonulin, a newly discovered modulator of intestinal permeability, and its expression in coeliac disease. *Lancet*. 2000;355(9214):1518–1519.
19. Fasano A. Regulation of intercellular tight junctions by zonula occludens toxin and its eukaryotic analogue zonulin. *Ann N Y Acad Sci*. 2000;915:214–222.
20. Wang W, et al. Human zonulin, a potential modulator of intestinal tight junctions. *J Cell Sci*. 2000;113 Pt 24:4435–4440.
21. Fasano A. All disease begins in the (leaky) gut: role of zonulin-mediated gut permeability in the pathogenesis of some chronic inflammatory diseases. *F1000Res*. 2020;9:69.
22. Drago S, et al. Gliadin, zonulin and gut permeability: Effects on celiac and non-celiac intestinal mucosa and intestinal cell lines. *Scand J Gastroenterol*. 2006;41(4):408–419.
23. Wyatt J, et al. Intestinal permeability and the prediction of relapse in Crohn's disease. *Lancet*. 1993;341(8858):1437–1439.
24. Noval Rivas M, et al. Intestinal permeability and IgA provoke immune vasculitis linked to cardiovascular inflammation. *Immunity*. 2019;51(3):508–521.
25. Ogata AF, et al. Ultra-sensitive serial profiling of SARS-CoV-2 antigens and antibodies in plasma to understand disease progression in COVID-19 patients with severe disease [posted online September 8, 2020]. *Clin Chem*. https://doi.org/10.1093/clinchem/hvaa213.
26. Krakauer T. Staphylococcal superantigens: pyrogenic toxins induce toxic shock. *Toxins (Basel)*. 2019;11(3):178.
27. Ramaswamy A, et al. Immune dysregulation and autoreactivity correlate with disease severity in SARS-CoV-2-associated multisystem inflammatory syndrome in children. *Immunity*. 2021;54(5):1083–1095.
28. Blanco-Melo D, et al. Imbalanced host response to SARS-CoV-2 drives development of COVID-19. *Cell*. 2020;181(5):1036–1045.
29. Mestecky J. *Mucosal Ommunology*. Elsevier Academic Press; 2005.
30. Norman M, et al. Ultrasensitive high-resolution profiling of early seroconversion in patients with COVID-19. *Nat Biomed Eng*. 2020;4(12):1180–1187.
31. Ouldali N, et al. Association of intravenous immunoglobulins plus methylprednisolone vs immunoglobulins alone with course of fever in Multisystem Inflammatory Syndrome in Children. *JAMA*. 2021;325(9):855–864.
32. Gopalakrishnan S, et al. Larazotide acetate promotes tight junction assembly in epithelial cells. *Peptides*. 2012;35(1):95–101.
33. Gopalakrishnan S, et al. Larazotide acetate regulates epithelial tight junctions in vitro and in vivo. *Peptides*. 2012;35(1):86–94.
34. Paterson BM, et al. The safety, tolerance, pharmacokinetic and pharmacodynamic effects of single doses of AT-1001 in coeliac disease subjects: a proof of concept study. *Aliment Pharmacol Ther*. 2007;26(5):757–766.
35. Leffler DA, et al. Larazotide acetate for persistent symptoms of celiac disease despite a gluten-free diet: a randomized controlled trial. *Gastroenterology*. 2015;148(7):1311–1319.
36. Massachusetts Department of Public Health. COVID-19 Response Reporting. https://www.mass.gov/info-details/covid-19-response-reporting. Updated May 20, 2021. Accessed

May 20, 2021.
37. Arad G, et al. Binding of superantigen toxins into the CD28 homodimer interface is essential for induction of cytokine genes that mediate lethal shock. *PLoS Biol*. 2011;9(9):e1001149.
38. Zhang W, et al. Molecular and serological investigation of 2019-nCoV infected patients: implication of multiple shedding routes. *Emerg Microbes Infect*. 2020;9(1):386–389.
39. Xiao F, et al. Evidence for gastrointestinal infection of SARS-CoV-2. *Gastroenterology*. 2020;158(6):1831–1833.
40. Jin X, et al. Epidemiological, clinical and virological characteristics of 74 cases of coronavirus-infected disease 2019 (COVID-19) with gastrointestinal symptoms. *Gut*. 2020;69(6):1002–1009.
41. El Asmar R, et al. Host-dependent zonulin secretion causes the impairment of the small intestine barrier function after bacterial exposure. *Gastroenterology*. 2002;123(5):1607–1615.
42. Thomas KE, et al. Gliadin stimulation of murine macrophage inflammatory gene expression and intestinal permeability are MyD88-dependent: role of the innate immune response in Celiac disease. *J Immunol*. 2006;176(4):2512–2521.
43. Fasano A. Intestinal permeability and its regulation by zonulin: diagnostic and therapeutic implications. *Clin Gastroenterol Hepatol*. 2012;10(10):1096–1100.
44. Fasano A. Zonulin and its regulation of intestinal barrier function: the biological door to inflammation, autoimmunity, and cancer. *Physiol Rev*. 2011;91(1):151–175.
45. Fabi M, et al. Gastrointestinal presentation of Kawasaki disease: a red flag for severe disease? *PLoS One*. 2018;13(9):e0202658.
46. Redd AD, et al. Microbial translocation, the innate cytokine response, and HIV-1 disease progression in Africa. *Proc Natl Acad Sci U S A*. 2009;106(16):6718–6723.
47. Camilleri M. Leaky gut: mechanisms, measurement and clinical implications in humans. *Gut*. 2019;68(8):1516–1526.
48. Consiglio CR, et al. The immunology of Multisystem Inflammatory Syndrome in Children with COVID-19. *Cell*. 2020;183(4):968–981.
49. Hennon TR, et al. COVID-19 associated multisystem inflammatory syndrome in children (MIS-C) guidelines; a Western New York approach. *Prog Pediatr Cardiol*. 2020;101232.
50. Rivnak AJ, et al. A fully-automated, six-plex single molecule immunoassay for measuring cytokines in blood. *J Immunol Methods*. 2015;424:20–27.
51. Edwards A, Haas W. Multiplexed quantitative proteomics for high-throughput comprehensive proteome comparisons of human cell lines. *Methods Mol Biol*. 2016;1394:1–13.
52. Hughes CS, et al. Single-pot, solid-phase-enhanced sample preparation for proteomics experiments. *Nat Protoc*. 2019;14(1):68–85.
53. Li J, et al. TMTpro reagents: a set of isobaric labeling mass tags enables simultaneous proteome-wide measurements across 16 samples. *Nat Methods*. 2020;17(4):399–404.
54. Lapek JD Jr, et al. Detection of dysregulated protein-association networks by high-throughput proteomics predicts cancer vulnerabilities. *Nat Biotechnol*. 2017;35(10):983–989.
55. Ting L, et al. MS3 eliminates ratio distortion in isobaric multiplexed quantitative proteomics. *Nat Methods*. 2011;8(11):937–940.
56. McAlister GC, et al. MultiNotch MS3 enables accurate, sensitive, and multiplexed detection of differential expression across cancer cell line proteomes. *Anal Chem*. 2014;86(14):7150–7158.
57. Erickson BK, et al. Evaluating multiplexed quantitative phosphopeptide analysis on a hybrid quadrupole mass filter/linear ion trap/orbitrap mass spectrometer. *Anal Chem*. 2015;87(2):1241–1249.
58. Erickson BK, et al. Active instrument engagement combined with a real-time database search for improved performance of sample multiplexing workflows. *J Proteome Res*. 2019;18(3):1299–1306.
59. Eng JK, et al. An approach to correlate tandem mass spectral data of peptides with amino acid sequences in a protein database. *J Am Soc Mass Spectrom*. 1994;5(11):976–989.
60. Huttlin EL, et al. A tissue-specific atlas of mouse protein phosphorylation and expression. *Cell*. 2010;143(7):1174–1189.
61. Elias JE, Gygi SP. Target-decoy search strategy for increased confidence in large-scale protein identifications by mass spectrometry. *Nat Methods*. 2007;4(3):207–214.
62. Crawford KHD, et al. Protocol and reagents for pseudotyping lentiviral particles with SARS-CoV-2 spike protein for neutralization assays. *Viruses*. 2020;12(5):513.
63. Ou X, et al. Characterization of spike glycoprotein of SARS-CoV-2 on virus entry and its immune cross-reactivity with SARS-CoV. *Nat Commun*. 2020;11(1):1620.
64. Ter-Ovanesyan D, et al. Ultrasensitive measurement of both SARS-CoV2 RNA and serology from saliva. *Anal Chem*. 2021;93(13):5365–5370.
65. CDC. CDC 2019-Novel Coronavirus [2019-NCoV] Real-Time RT-PCR Diagnostic Panel. https://www.fda.gov/media/134922/download. Updated December 1, 2020. Accessed May 20, 2021.
66. Lima R, et al. Establishment of a pediatric COVID-19 biorepository: unique considerations and opportunities for studying the impact of the COVID-19 pandemic on children. *BMC Med Res Methodol*. 2020;20(1):228.